This is the post-print version of the following communication: Nicoll Zeballos, Eleftheria Diamanti, Ana I. Benítez-Mateos, Claudia Schmidt-Dannert, and Fernando López-Gallego, Solid-Phase Assembly of Multienzyme Systems into Artificial Cellulosome, Bioconjugate Chem. 2021, 32, 9, 1966–1972

DOI: 10.1021/acs.bioconjchem.1c00327

Solid-phase assembly of multi-enzyme systems into artificial cellulosomes

Nicoll Zeballos[a], Eleftheria Diamanti[a], Ana I. Benítez-Mateos[a], Claudia Schmidt-Dannert[b] and Fernando López-Gallego[a,c,*]

[a]Heterogeneous Biocatalysis Laboratory, Center for Cooperative Research in Biomaterials (CIC biomaGUNE), Basque Research and Technology Alliance (BRTA), Paseo de Miramón 194, Donostia San Sebastián, Spain

[b]Department of Biochemistry, Molecular Biology and Biophysics, University of Minnesota, St. Paul, MN 55108, USA

[c]IKERBASQUE, Basque Foundation for Science, María Díaz de Haro 3, 48013 Bilbao, Spain

*Corresponding author:

Fernando López-Gallego: flopez@cicbiomagune.es

Keywords: Protein immobilization, biocascades, ω-transaminase, alcohol dehydrogenase

Abstract

We herein describe a bio-inspired solid-phase assembly of a multi-enzyme system scaffolded on an artificial cellulosome. An alcohol dehydrogenase and an ω-transaminase were fused to cohesin and dockerin domains to drive their sequential and ordered co-immobilization on agarose porous microbeads. The resulting immobilized scaffolded enzymatic cellulosome was characterized through quartz crystal microbalance with dissipation and confocal laser scanning microscopy to demonstrate that both enzymes interact with each other and physically colocalize within the microbeads. Finally, the assembled multi-functional heterogeneous biocatalyst was tested for the one-pot conversion of alcohols into amines. Using the physically co-localized enzymatic system confined into porous microbeads, the yield of the corresponding amine was 1.3 and 10 times higher than the spatially segregated immobilized system and the free enzymes, respectively. This work establishes the basis of a new concept to organize multi-enzyme systems at the nanoscale within solid and porous immobilization carriers.

Multi-enzyme systems are gaining momentum for chemical manufacturing as they allow executing complex synthetic routes to yield highly pure products without requiring intermediate purification and protection/deprotection steps.[1] The simultaneous operation of several enzymes can also increase the overall production yield and system efficiency by pulling the cascade towards the final product while preventing the accumulation of potentially toxic and inhibitory intermediates.[2] Achieving high fluxes through a biocatalytic cascade though, requires optimal coupling of enzyme reactions.[3] Biological living systems orchestrate fluxes of biosynthetic pathways through a variety of mechanisms including e.g. gene regulation,[4] allosteric control[5] and spatial compartmentalization[6] of enzyme activities; strategies which have been adopted for cellular engineering of metabolic pathways.[7] Far fewer approaches and tools are available for the efficient orchestration of enzyme cascades in cell-free (*in vitro)* reactions. *In vitro* synthetic biology or cell-free metabolic engineering is an emerging approach aimed at assembling artificial biosynthetic cascades using isolated enzymes. Such *in vitro* systems can operate under non-physiological conditions and are unimpeded by mass transfer, inhibitory (e.g. high substrate concentration, toxic reaction compounds) and side reaction issues, common to cellular systems. Cell-free operation also allows for the rapid proto-typing of cascades and isolation of purer products.[8, 9]

A major drawback of cell-free reactions is that they are based on isolated enzymes working under dilute conditions rather than the crowded and spatially organized environment of cells. [10] Several groups including ours, have successfully demonstrated confinement and co-immobilization of enzyme cascades on solid materials.[11-13] These co-localization strategies, however, lack the precision required to organize biocatalysts at the nanometre scale afforded by the biological systems. Different self-assembling supramolecular structures have been fabricated based on protein,[14, 15] DNA/RNA[16] or nanoparticle [17] building blocks to which target enzymes are attached via genetic fusions, engineered interaction domains or chemical

modification. Such scaffolding approaches were shown to enhance the reaction efficiency of the multi-enzyme systems for chemical synthesis.[18]

Nature employs its own supramolecular scaffolds to organize enzymes into metabolomes. One such type of metabolome is the bacterial cellulosome that co-localizes and positions a cohort of glycosidases at the extracellular membrane for the degradation of the recalcitrant plant cell wall polymer cellulose.[19] Cellulosomes have highly modular architectures where a scaffoldin protein anchored to the cell wall displays cohesin (Coh) domains to which secreted glycosidases attach via cognate dockerin (Doc) domains. Binding of the metabolomes to cellulose is facilitated by cellulose binding domains. Inspired by their plug-and-play organization, synthetic cellulosomes have been engineered mostly for cell-based applications in biorefinery processes.[20-23] For *in vitro* applications, mini-cellulosomes have been designed for the selective assembly of multi-enzyme systems through the calcium-dependent interactions of Coh/Doc pairs, enhancing the efficiency of several chemical manufacturing cascades.[14, 24-28] These mini-cellulosomes have also been immobilized on cellulose-based or cellulose-coated solid materials for recycling.[14] However, the structural diversity of such engineered cellulosome scaffolds used to organize multi-enzyme systems in the space is limited by the low number of available highly specific Coh/Doc pairs. Another challenge is the cellulosome assembly using large and/or multimeric enzymes causing molecular crowding and steric hindrances.[29] In this study we sought to develop an alternative strategy where we use porous agarose microbeads for the construction of a cellulosome inspired, artificial metabolome (dubbed immobilized scaffolded enzymatic cellulosome or short, iSECel) that is genetically programmable. A similar approach was exploited to create polyproteams using monomeric affibodies tagged with the spy and snoop tag/catcher systems for cell-signalling,[30] but never intended with the cellulosome architecture for applied biocatalysis.

As a model system, we spatially organized a two-step cascade for one-pot transformation of alcohols into amines concurrently catalyzed by a NADH-dependent alcohol dehydrogenase (ADH) and an ω-transaminase (ωTA). We orderly assembled our dual enzyme system in solid phase (porous microbeads) by sequential binding of Coh/Doc pairs genetically fused to recombinant enzymes **(**Figure 1**).**

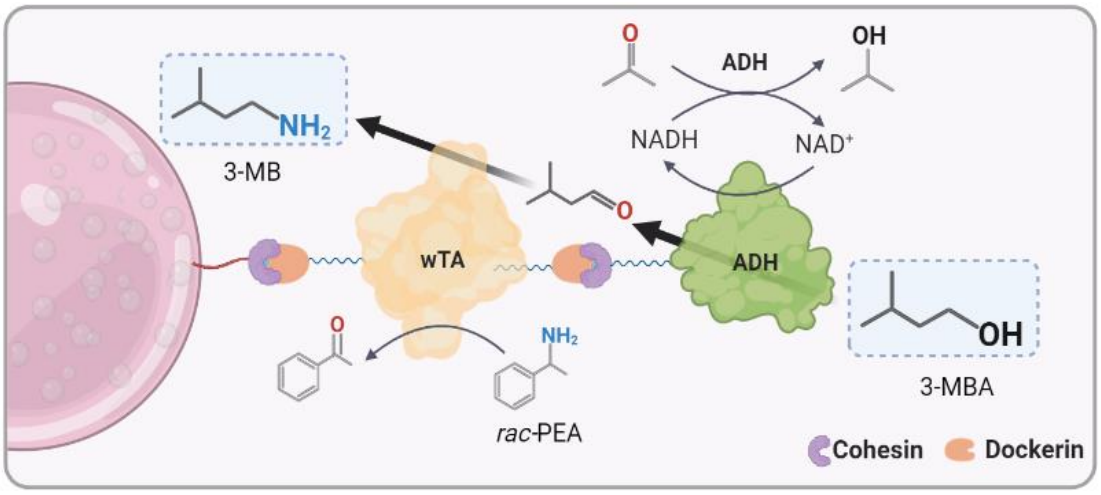

Figure 1. Schematic representation of the immobilized scaffolded enzymatic cellulosome (iSECel) assembled in solid phase. Porous agarose microbeads (pink) functionalized with cobalt chelating groups bind His-tagged Coh domains as priming units to which enzymes are bound via cognate Dock domains as shown. ωTA: ω-transaminase. ADH: Alcohol dehydrogenase. For clarity purposes the quaternary structures of the enzymes are omitted in the iSECel representation.

From the increasing number of described Coh/Doc pairs, we chose the well-characterized type II Coh/Doc pair from *Clostridium thermocellum*.[31, 32] The 20 kDa Coh domain was fused to the N-terminus of a tetrameric ADH from *Bacillus (Geobacillus) stearothermophilus*[33] (~56 kDa monomer of C-ADH), while the 18 kDa Doc domain was fused to both the N- and C-terminus of a dimeric PLP-dependent (*R*)-ωTA from *Aspergillus terreus*[34] (~74 kDa monomer of D-ωTA-D) (structures shown in Figure S1). As a proxy element for D-ωTA-D, we also fused Coh domains to both termini of a monomeric enhanced cyan fluorescent protein (~68 kDa D-ECFP-

D). Furthermore, flexible GS-linkers were inserted between the cellulosome domains and the enzymes to reduce potential steric hindrances during the interaction (Table S1). The presumed multimeric fusion protein complexes therefore display 4 Doc (~148 kDa D-ωTA-D dimer) and 4 Coh (~226 kDa C-ADH tetramer) sites for the interaction with their cognate binding domains. Finally, to prime the solid-phase assembly of the iSECel, we fused a 6xHis-tag to the C-terminus of the Coh domain (~ 21 kDa C-His) for its binding to agarose porous microbeads functionalized with cobalt chelates (AG-Co^{2+}). Each modified protein was overexpressed in *E. coli* BL21(DE3) cells and their corresponding cell-free protein extracts were incubated with AG-Co^{2+} microbeads. The binding selectivity and strong affinity of the Coh/Doc interaction enables solid-phase assembly of the iSECel system directly from crude cell lysates using therefore non-purified enzymes. In three sequential steps, microbeads were first incubated with C-His and then followed by incubations with D-ωTA-D and C-ADH. In our iSECel system, the enzymes themselves are part of the scaffolding (Figure 1) unlike other reported mini-cellulosome systems.[20]

To test and optimize the assembly of our iSECel system, we first incubated D-ωTA-D with AG-Co^{2+} functionalized with C-His in presence of 1 mM $CaCl_2$. Herein, we demonstrated that D-ωTA-D is immobilized on microbeads functionalized with C-His, but not on naked ones (Figure S2). We obtained similar results with the monomeric D-ECFP-D, suggesting that this method will also work for other proteins (Figure S3). Next, we investigated the effect of C-His functionalization density (i.e., load) on the D-ωTA-D immobilization efficiency. To do this, we incubated AG-Co^{2+} with different concentrations of purified C-His, offering 1.8 to 3.7 mg of C-His per gram of solid, achieving a quantitative immobilization yield in both cases. The functionalized microbeads were then incubated with equal and consecutive amounts of D-ωTA-D and C-ADH cell-free extracts and the immobilized complexes were analyzed by SDS-PAGE and quantified by densitometry (Figure 2A).[35] First, SDS-PAGE analysis confirmed

successful solid-phase assembly of the iSECel system as all protein units were disassembled and desorbed from the microbeads under denaturing conditions. Second, we found that the immobilization yield of both D-ωTA-D and C-ADH minimally increased at higher C-His functionalization density. Therefore, the assembly efficiency of iSECel was already maximal at the lowest C-His load (1.8 mg C-His x g^{-1} microbeads) herein tested. These results suggest that the iSECel assembly is limited by the density and the crowding of the Coh priming unit at the surface of the AG-Co^{2+}. Similar insights were found with mini-cellulosomes displayed on yeast cells surfaces, where molecular crowding was shown to limit multi-enzyme assembly efficiency.[29] To confirm that C-ADH was selectively bound to D-ωTA-D towards a Coh/Dock interaction, we constructed a mCherry fluorescence variant whose N-terminus was fused to the Dock domain (D-mCherry) to perform competitive assays. When D-mCherry was incubated with the iSECel in presence of calcium chloride, C-ADH was quantitatively released from the resin. These results indicate that the excess of D-mCherry binds C-ADH, competing with the assembled D-ωTA-D for the binding of C-ADH, and thus displacing the latter from the iSECel (Figure S4B). Herein, we demonstrate that D-ωTA-D selectively captures C-ADH through a Dock/Coh interaction.

Quantification of protein bands by densitometry estimated a mass ratio of 1.1:1.3:1 for C-His:D-ωTA-$D_{(2\text{-mer})}$:C-$ADH_{(4\text{-mer})}$ (corresponding to a molar ratio of 12:2:1) at the microbead surface (Table S2). These ratios reflect the size differences of the monomeric (C-His) and quaternary structures of the interacting enzymes in the iSECel. In this supramolecular assembly, each C-ADH tetramer (4 Coh domains) appears to be attached to two D-ωTA-D dimmers (4 Doc domains). We noted that the assembled iSECel could not be eluted from the microbeads upon incubation with imidazole and only harsh denaturing conditions used for SDS-PAGE analysis were capable to disassemble the scaffolded multi-enzyme system (Figure

S4A). This insight suggests a dense coverage of the microbeads and strong multivalent interactions between Coh and Doc domains of the assembled proteins.

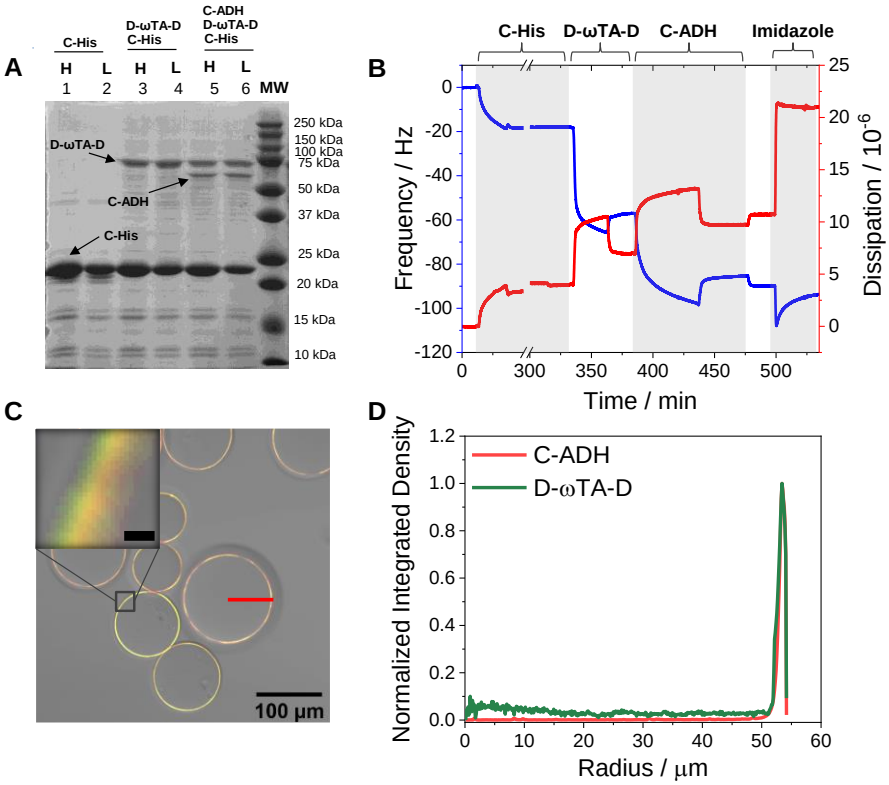

Figure 2. (A) SDS-PAGE analysis of proteins attached to AG-Co^{2+} microbeads after each assembly step. Lane 1 and 2 show C-His release upon the first assembly step. Lanes 3 and 4 show C-His and D-ωTA-D release upon the second assembly step. Lanes 5 and 6 show C-His, D-ωTA-D and C-ADH release upon the third assembly step. Lanes H and L show the system assembled with the highest (1.8 $mg_{C\text{-}His}$ x g^{-1}_{resin}) and lowest (3.7 $mg_{C\text{-}His}$ x g^{-1}_{resin}) load of C-His, respectively. Lane MW: Molecular weight marker. (B) Real-time QCM-D measurements of the sequential assembly of C-His, D-ωTA-D and C-ADH on Co^{2+} functionalized quartz crystal surface. Imidazole means a 0.5 M imidazole wash. (C) Co-localization of D-ωTA-D (green: fluorescein labelled) and C-ADH (red: rhodamine labelled) on C-His functionalized microbeads (50-150 µm diameter) by CLSM. Red line depicts the radial cross-section of one selected microbead. Top left inset is the magnification of the outer surface of the microbead; scale (black line) is 0.5 µm. (D) Average (n = 10) radial cross-section fluorescence profile of D-ωTA-D and C-ADH co-immobilized on AG-Co^{2+} microbeads (for more details see Figure S5).

To further characterize iSECel assembly in more detail, we monitored the sequential iSECel assembly by QCM-D (quartz crystal microbalance with dissipation) on cobalt chelate functionalized silicon surfaces following the same stepwise protocol used for microbeads functionalization (Figure 2B). Each adsorption step decreases the frequency (increment in mass deposition) and increases the energy dissipation factor (increase of surface viscoelasticity) of the system. Frequency changes reflected the adsorption of C-His (Δf=17.7 Hz) onto the sensor surface and the subsequent binding of D-ωTA-D (Δf=39.3 Hz) and C-ADH (Δf=28.7 Hz). Larger frequency changes correspond to higher mass adsorption, pointing out that the calculated mass ratio of the adsorbed C-His: D-ωTA-D:C-ADH (0.6:1.4:1) through QCM-D were similar to that ratio obtained by SDS-PAGE densitometry (1.1:1.3:1)) (Table S2). Upon iSECel assembly, the total differences in frequency and energy dissipation (Δf= 85.7 Hz and $\Delta D = 9.69 \times 10^{-6}$) confirm the adsorption of a large macromolecular complex and the formation of a soft hydrated film. Remarkably, rinsing the sensor surface with 0.5 M imidazole caused only a small decrease in frequency (Δf= 4.23 Hz), confirming the results obtained with microbeads upon imidazole elution. We then performed the iSECel assembly with fluorescently labelled D-ωTA-D and C-ADH to analyse their spatial location within the microbeads by confocal laser scanning microscopy (CLSM) (Figure 2C). Both enzymes occupied the outer surface of the microbeads, representing 4.45±1.56 % of the particle radius (Figure 2D). Quantitative image analysis confirmed that 93% of the two enzymes co-localized at the outer 3-4 µm of the microbeads according to Pearson´s coefficient (Table S3).[36]

After characterizing iSECel solid-phase assembly, we next determined the immobilization parameters for each enzyme during the iSECel assembly using colorimetric assays (Table 1).

About 90% of the D-ωTA-D activity (immobilization yield Ψ%) in the cell-free extract was bound to the microbeads activated with C-His. 89 % of loaded D-ωTA-D was active upon attachment to the microbeads, recovering an activity of 0.51 U g^{-1} of microbeads. Subsequent attachment of C-ADH achieved a 35% immobilization yield, but the immobilized enzyme recovered only 6 % of the loaded activity (corresponding to 0.033 U g^{-1} of microbeads) upon immobilization. While the activity of D-ωTA-D was only slightly reduced upon assembly (0.44 U g^{-1}), the activity of C-ADH was significantly reduced once assembled into the iSECel (Table 1).

Table 1. Apparent activity of the enzymes assembled in the iSECel

Assembly Product	Enzyme	[a]Ψ %	[b]Load (U/g)	[c]RA (U/g) (%)
Co-localized iSECel (His-C/D-ωTA-D/C-ADH)	ωTA	89 ± 0.3	[d] 0.61± 0.01	[d] 0.44 ± 0.03 (72)
	ADH	35 ± 4	[d] 0.52±0.06	[d] 0.033 ± 0.003(6)
Segregated iSECel (His-C/D-ωTA-D + His-C/D-ECFP-D/C-ADH)	ωTA	89 ± 0.3	[d] 0.61±0.01	[d] 0.51 ± 0.05 (84)
	ADH	36 ± 7	[d] 0.41±0.08	0.18 ± 0.08 (44)

a. Immobilization yield (Ψ) % = (100 – ((Activity remaining in supernatant after immobilization / Activity in cell-free extract prior to immobilization) x 100).

b. Load represents the theoretically immobilized activity per gram of microbeads according to Ψ and considering the offered activity per gram of carrier. Free enzyme lysates kept 100% activity under the immobilization conditions.

c. Recovered activity (RA) is the measured activity per gram of microbeads after immobilization. The relative recovered activity (%) is the percentage of the loaded activity recovered after the immobilization (% RA = (RA/Load) x 100).

All mean values are the averages of three replicates with their corresponding standard deviation (SD).

d. SD lower than the 5% of the mean value.

In contrast, C-ADH was 8 times more active using D-ECFP-D as a proxy for D-ωTA-D despite both Dock cognates immobilized similar C-ADH yields (Table 1). Unlike the monomeric D-ECFP-D (68 kDa), the bulkier dimmer D-ωTA-D (148 kDa) may promote a more crowded iSECel within the agarose pores that might induce conformational changes in ADH structure and/or impede the diffusion of co-factors/substrates towards its active site. We previously observed a similar activity reduction for this enzyme when co-immobilized with three other enzymes on porous microbeads.[12] The final ratio of activity of C-ADH: D-ωTA-D immobilized on the co-localized iSECel is 1:13 despite their 1:2 molar ratio, indicating that the alcohol oxidation will likely be the rate limiting step of this cascade.

Once the activities of the two enzymes in the iSECel were confirmed, we applied this dual enzyme cascade for the one-pot, two step biotransformation of 3-methyl-1-butanol (3-MB) into 3-methyl-1-butylamine (3-MBA) (Figure 1). As auxiliary co-substrates, we used acetone as electron acceptor to regenerate NAD^+ for ADH catalysis and *rac*-phenylethylamine (*rac*-PEA) as amine donor to shift the transaminase reaction equilibrium towards the amine formation. We determined that the scaffolded C-ADH catalyses the reduction of the co-substrate acetone 13 times faster than the oxidation of 3-MB (Table S4) thereby ensuring efficient NAD^+ co-factor regeneration for the first step of the biotransformation. We then established that acetone is not a suitable substrate for the scaffolded D-ωTA-D (Table S4) and therefore does not compete with the aldehyde intermediate of the cascade reaction. Therefore, during the concurrent transamination reaction, the *R*-selective D-ωTA-D transfers the amine group of *R*-1-phenylethyl amine (PEA) of the racemic co-substrate only to the aldehyde intermediate to yield 3-MBA and acetophenone as only products. When the iSECel was incubated for 24 hrs (pH 7, 30 °C, 250 rpm) with 10 mM of 3-MB, 0.5 mM of NAD^+, 100 mM of acetone and 2 mM of *rac*-PEA, we obtained 0.69 ± 0.1 mM 3-MBA, representing 69% of the maximum theoretical conversion as the enantioselective D-ωTA-D only utilizes the half (R-isomer) of the amine

donor *rac*-PEA (Figure S6). The overall iSECel catalyst productivity, in batch, was 4.4 nmol of 3-MBA min^{-1} g^{-1} under the conditions described above.

To demonstrate that the physical proximity of both C-ADH and D-ωTA-D enhances the overall efficiency of the biocascade, we separately immobilized both enzymes through Coh/Dock interactions on two different microbeads of AG-Co^{2+}. To that aim D-ωTA-D was immobilized on one single microbead functionalized with C-His, while C-ADH was immobilized on a different one functionalized with the complex His-C/D-ECFP-D. Even though C-ADH was more active when immobilized by its own (Table 1), the segregated system yielded 30% less 3-MBA (0.53 ± 0.05 mM) than the co-localized one. In contrast, the free multi-enzyme system only reached 7% of the theoretical conversion (0.07±0.01 mM) (Table S5).

The acetophenone production courses of the two-step oxidative amination catalyzed by iSECel with different spatial organization confirm that co-localized iSECel catalyses the step-wise transformation of 3-MB to 3-MBA more efficiently than the two enzymes separately immobilized on AG-Co^{2+} (segregated iSECel) (Figure 3A). Furthermore, we observed no lag time in the acetophenone production when using co-localized iSECel unlike in the cascade performed with the segregated iSECel. The absence of lag phase in cascade reactions is one of the sings of substrate channelling,[37] supporting the physical proximity of the two enzymes in the co-localized iSECel architecture. The fact that these two enzymes are linked through supramolecular Coh/Dock interactions within the intraporal space of the agarose beads may maximize the transport efficiency of the aldehyde intermediate from the C-ADH to the D-ωTA-D.

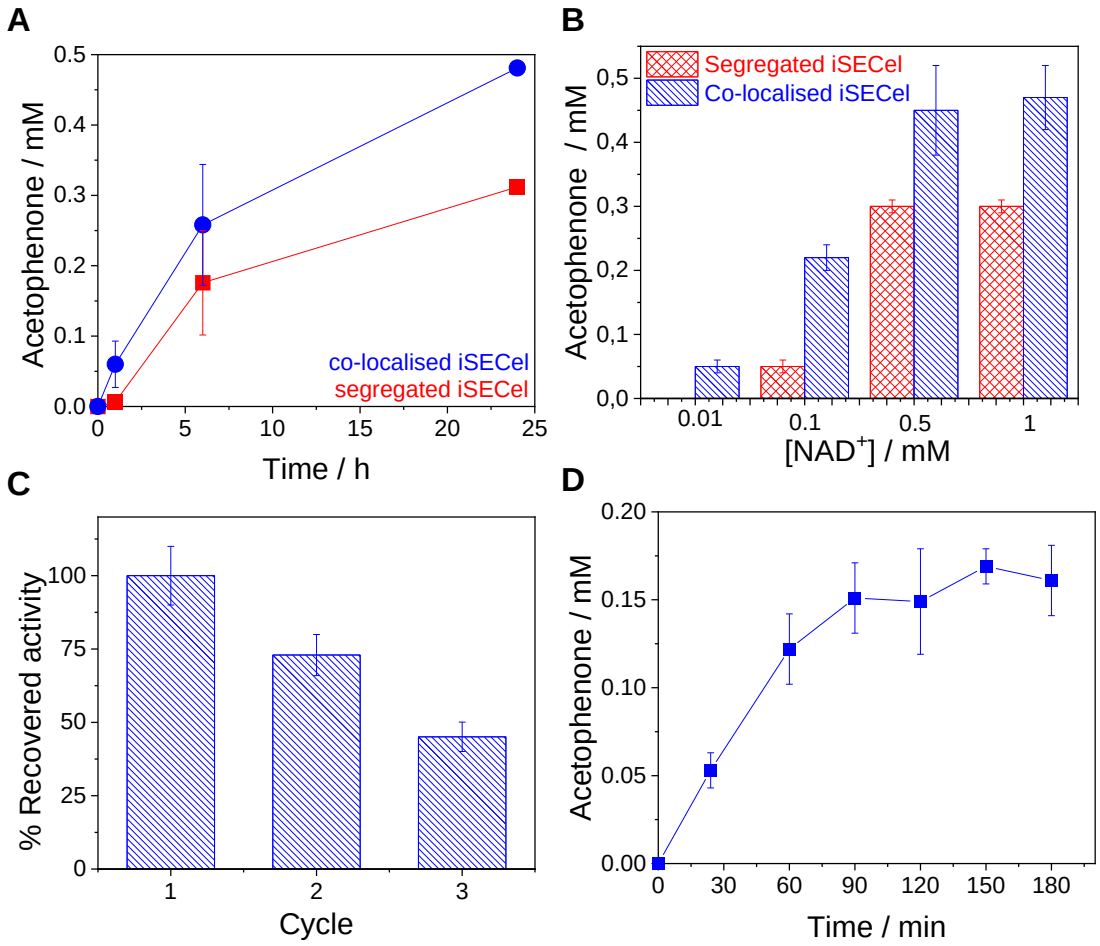

Figure 3. (A) Reaction course of the oxidative amination of 3-MB into 3-MBA by monitoring the acetophenone titre during the biotransformation catalyzed by iSECels with different spatial organization. (B) Acetophenone produced after 24 h at different NAD^+ concentrations. (C) Recycling of co-localized iSECel in consecutive batch cycles (D). Continuous reaction performed by co-localized iSECel packed into a plug-flow column at 10 µL x min^{-1} flow rate. In all panels, co-localized iSECels and segregated iSECels are shown as blue and red lines and bars, respectively. All reactions were performed in 10 mM of 3-MB and 1 mM of rac-PEA with 0.5 mM NAD^+ but in panel B, where NAD^+ concentrations varied. Plotted data are the mean values of three replicates with their corresponding standard deviation (error bars).

Furthermore, the co-localized iSECel yielded 1.5 and 4 times higher acetophenone titres than the segregated iSECel system using 0.5 and 0.1 mM NAD^+, respectively (Figure 3B). At low NAD^+ concentrations, less aldehyde is produced by ADH and its transport to the physically segregated ωTA microbeads becomes rate-limiting. In contrast, the physical proximity in the

co-immobilized iSECel does not have that limitation. Therefore, the intermediate utilization was more efficient when the two enzymes were assembled into the synthetic cellulosome and co-immobilized on the same microbead. Such difference was more drastic at NADH concentration as low as 0.01 mM where acetophenone was only detected when iSECel was used. Similar effects were reported for a comparable enzyme cascade co-immobilized on porous agarose microbeads for the conversion of diols into aminoalcohols.[12]

Finally, we tested the reusability of our iSECel dual enzyme system. Figure 3C shows that the multi-enzyme system can be recycled in batch, but its overall operational activity is reduced by 60% after 3 reaction cycles. To further expand the application of our system, we integrated the iSECel into a plug-flow column for continuous transformation of 3-MB into 3-MBA. Figure 3D demonstrates that iSECel catalyst can operate in flow with a maximum production rate of 8 nmol of 3-MBA x min^{-1} x $g_{carrier}^{-1}$, representing 2-times higher specific productivity than the batch operated system.

Conclusions

In summary, we have developed a genetically programmable solid-phase enzyme assembly system and demonstrated its use with a dual enzyme cascade for amination of alcohols. This work has pioneered the use of this convoy-like approach for the orderly co-immobilization of multimeric enzymes and their further use and recycling. Herein, we show that the nanometric proximity of the two orderly scaffolded enzymes in porous agarose microbeads enhances the heterogeneous cascade performance. Finally, we integrated our iSECel into a flow-reactor for continuous synthesis of 3-MBA. This work establishes the basis of a new concept to organize multi-enzyme systems at the nanoscale within solid matrices that can be readily expanded to other biocatalytic cascade reactions and enrich the toolbox for cell-free biotransformations.

Associated content

Supporting information

The Supporting Information is available free of charge at https://pubs.acs.org/doi

Materials and methods, protein sequences, SDS-PAGE analysis, activity assays and chromatographic methods.

Author information

Corresponding author

Fernando López-Gallego – *Heterogeneous Biocatalysis Laboratory, Center for Cooperative Research in Biomaterials (CIC biomaGUNE), Basque Research and Technology Alliance (BRTA), Paseo de Miramón 194, Donostia San Sebastián, Spain.*

IKERBASQUE, Basque Foundation for Science, María Díaz de Haro 3, 48013 Bilbao, Spain

ORCID: 0000-0003-0031-1880

e-mail: flopezicbiomagune.es

Authors:

Nicoll Zeballos - *Heterogeneous Biocatalysis Laboratory, Center for Cooperative Research in Biomaterials (CIC biomaGUNE), Basque Research and Technology Alliance (BRTA), Paseo de Miramón 194, Donostia San Sebastián, Spain*

Eleftheria Diamanti - *Heterogeneous Biocatalysis Laboratory, Center for Cooperative Research in Biomaterials (CIC biomaGUNE), Basque Research and Technology Alliance (BRTA), Paseo de Miramón 194, Donostia San Sebastián, Spain*

Ana I. Benítez-Mateos - *Heterogeneous Biocatalysis Laboratory, Center for Cooperative Research in Biomaterials (CIC biomaGUNE), Basque Research and Technology Alliance (BRTA), Paseo de Miramón 194, Donostia San Sebastián, Spain*

University of Bern, 3012 Bern, Switzerland

ORCID:0000-0001-6948-7652

Claudia Schmidt-Dannert - *Department of Biochemistry, Molecular Biology and Biophysics, University of Minnesota, St. Paul, MN 55108, USA*

ORCID: 0000-0002-0559-3656

Notes

The authors declare no conflicts of interest.

Acknowledgements

All authors acknowledge funding from Spanish Government (BIO2015-69887-R, RTI2018-094398-B-I00 and MDM-2017-0720). FLG thanks the funding of IKERBASQUE.

Abbreviations

3-methyl-1-butanol (3-MB), 3-methyl-1-butylamine (3-MBA), alcohol dehydrogenase (ADH), agarose porous microbeads functionalized with cobalt chelates (AG-Co^{2+}), cohesin (Coh), confocal laser scanning microscopy (CLSM), dockerin (Doc), enhanced cyan fluorescent protein (ECFP), immobilized scaffolded enzymatic cellulosome (iSECel), *rac*-phenylethylamine (*rac*-PEA), quartz crystal microbalance with dissipation (QCM-D) and ω-transaminase (ωTA).

References

(1)Wu, S.; Snajdrova, R.; Moore, J. C.; Baldenius, K.; Bornscheuer, U. T., Biocatalysis: Enzymatic Synthesis for Industrial Applications. *Angew. Chem. Int. Ed.* (2020)**,** *60*, 88-119.
(2)Fessner, W. D., Systems Biocatalysis: Development and engineering of cell-free "artificial metabolisms" for preparative multi-enzymatic synthesis. *New Biotechnol.* (2015)**,** *32*, 658-64.
(3)Schmidt-Dannert, C.; Lopez-Gallego, F., A roadmap for biocatalysis - functional and spatial orchestration of enzyme cascades. *Microb. Biotechnol.* (2016)**,** *9*, 601-609.
(4)Carthew, R. W., Gene Regulation and Cellular Metabolism: An Essential Partnership. *Trends Genet.* (2020).

(5)Lisi, G. P.; Loria, J. P., Allostery in enzyme catalysis. *Curr. Opin. Struct. Biol.* (2017)**,** *47*, 123-130.
(6)Schmitt, D. L.; An, S., Spatial Organization of Metabolic Enzyme Complexes in Cells. *Biochemistry* (2017)**,** *56*, 3184-3196.
(7)Avalos, J. L.; Fink, G. R.; Stephanopoulos, G., Compartmentalization of metabolic pathways in yeast mitochondria improves the production of branched-chain alcohols. *Nat. Biotechnol.* (2013)**,** *31*, 335-341.
(8)Ullah, M. W.; Khattak, W. A.; Ul-Islam, M.; Khan, S.; Park, J. K., Metabolic engineering of synthetic cell-free systems: Strategies and applications. *Biochem. Eng. J.* (2016)**,** *105*, 391-405.
(9)Burgener, S.; Luo, S.; McLean, R.; Miller, T. E.; Erb, T. J., A roadmap towards integrated catalytic systems of the future. *Nat. Catal.* (2020)**,** *3*, 186-192.
(10)Küchler, A.; Yoshimoto, M.; Luginbühl, S.; Mavelli, F.; Walde, P., Enzymatic reactions in confined environments. *Nat. Nanotechnol.* (2016)**,** *11*, 409.
(11)Li, Z.; Zhang, Y.; Su, Y.; Ouyang, P.; Ge, J.; Liu, Z., Spatial co-localization of multi-enzymes by inorganic nanocrystal-protein complexes. *Chem. Commun.* (2014)**,** *50*, 12465-8.
(12)Velasco-Lozano, S.; Santiago-Arcos, J.; Mayoral, J. A.; López-Gallego, F., Co-immobilization and Colocalization of Multi-Enzyme Systems for the Cell-Free Biosynthesis of Aminoalcohols. *ChemCatChem* (2020)**,** *12*, 3030-3041.
(13)Vázquez-González, M.; Wang, C.; Willner, I., Biocatalytic cascades operating on macromolecular scaffolds and in confined environments. *Nat. Catal.* (2020)**,** *3*, 256-273.
(14)You, C.; Zhang, Y. H., Self-assembly of synthetic metabolons through synthetic protein scaffolds: one-step purification, co-immobilization, and substrate channeling. *ACS Synth. Biol.* (2013)**,** *2*, 102-10.
(15)Kang, W.; Ma, T.; Liu, M.; Qu, J.; Liu, Z.; Zhang, H.; Shi, B.; Fu, S.; Ma, J.; Lai, L et al., Modular enzyme assembly for enhanced cascade biocatalysis and metabolic flux. *Nat. Comm.* (2019)**,** *10*, 4248.
(16)Wang, C.; Yue, L.; Willner, I., Controlling biocatalytic cascades with enzyme–DNA dynamic networks. *Nat. Catal.* (2020)**,** *3*, 941-950.
(17)Vranish, J. N.; Ancona, M. G.; Oh, E.; Susumu, K.; Lasarte Aragonés, G.; Breger, J. C.; Walper, S. A.; Medintz, I. L., Enhancing Coupled Enzymatic Activity by Colocalization on Nanoparticle Surfaces: Kinetic Evidence for Directed Channeling of Intermediates. *ACS Nano* (2018)**,** *12*, 7911-7926.
(18)Ellis, G. A.; Klein, W. P.; Lasarte-Aragonés, G.; Thakur, M.; Walper, S. A.; Medintz, I. L., Artificial Multienzyme Scaffolds: Pursuingin VitroSubstrate Channeling with an Overview of Current Progress. *ACS Catal.* (2019)**,** *9*, 10812-10869.
(19)Artzi, L.; Bayer, E. A.; Moraïs, S., Cellulosomes: bacterial nanomachines for dismantling plant polysaccharides. *Nat. Rev. Microbiol.* (2017)**,** *15*, 83-95.
(20)Hu, B.-B.; Zhu, M.-J., Reconstitution of cellulosome: Research progress and its application in biorefinery. *Biotechnology and Applied Biochemistry* (2019)**,** *66*, 720-730.
(21)Fan, L.-H.; Zhang, Z.-J.; Yu, X.-Y.; Xue, Y.-X.; Tan, T.-W., Self-surface assembly of cellulosomes with two miniscaffoldins on *Saccharomyces cerevisiae* for cellulosic ethanol production. *Proc. Natl. Acad. Sci. USA* (2012)**,** *109*, 13260-13265.
(22)Liang, Y.; Si, T.; Ang, E. L.; Zhao, H., Engineered pentafunctional minicellulosome for simultaneous saccharification and ethanol fermentation in Saccharomyces cerevisiae. *Applied and environmental microbiology* (2014)**,** *80*, 6677-6684.
(23)Liu, F.; Banta, S.; Chen, W., Functional assembly of a multi-enzyme methanol oxidation cascade on a surface-displayed trifunctional scaffold for enhanced NADH production. *Chem. Commun.* (2013)**,** *49*, 3766-3768.
(24)Mori, Y.; Nakazawa, H.; Gonçalves, G. A. L.; Tanaka, T.; Umetsu, M.; Kamiya, N., One-dimensional assembly of functional proteins: toward the design of an artificial cellulosome. *Mol. Syst. Des. Eng.* (2016).
(25)Szczupak, A.; Aizik, D.; Moraïs, S.; Vazana, Y.; Barak, Y.; Bayer, E. A.; Alfonta, L., The Electrosome: A Surface-Displayed Enzymatic Cascade in a Biofuel Cell's Anode and a High-Density Surface-Displayed Biocathodic Enzyme. *Nanomaterials* (2017)**,** *7*, 153.

(26)Chen, H.; Huang, R.; Kim, E.-J.; Zhang, Y.-H. P. J., Building a Thermostable Metabolon for Facilitating Coenzyme Transport and In Vitro Hydrogen Production at Elevated Temperature. *ChemSusChem* (2018)**,** *11*, 3120-3130.
(27)Lu, J.; Zhang, Y.; Sun, D.; Jiang, W.; Wang, S.; Fang, B., The Development of Leucine Dehydrogenase and Formate Dehydrogenase Bifunctional Enzyme Cascade Improves the Biosynthsis of L-tert-Leucine. *Applied Biochemistry and Biotechnology* (2016)**,** *180*, 1180-1195.
(28)Meng, D.; Wu, R.; Wang, J.; Zhu, Z.; You, C., Acceleration of cellodextrin phosphorolysis for bioelectricity generation from cellulosic biomass by integrating a synthetic two-enzyme complex into an in vitro synthetic enzymatic biosystem. *Biotechnol. Biofuels* (2019)**,** *12*, 267.
(29)Smith, M. R.; Gao, H.; Prabhu, P.; Bugada, L. F.; Roth, C.; Mutukuri, D.; Yee, C. M.; Lee, L.; Ziff, R. M.; Lee, J.-K.; et al., Elucidating structure–performance relationships in whole-cell cooperative enzyme catalysis. *Nat. Catal.* (2019)**,** *2*, 809-819.
(30)Veggiani, G.; Nakamura, T.; Brenner, M. D.; Gayet, R. V.; Yan, J.; Robinson, C. V.; Howarth, M., Programmable polyproteams built using twin peptide superglues. *Proc. Natl. Acad. Sci. USA* (2016)**,** *113*, 1202-1207.
(31)Alves, V. D.; Fontes, C.; Bule, P., Cellulosomes: Highly Efficient Cellulolytic Complexes. *Subcell Biochem* (2021)**,** *96*, 323-354.
(32)Adams, J. J.; Pal, G.; Jia, Z.; Smith, S. P., Mechanism of bacterial cell-surface attachment revealed by the structure of cellulosomal type II cohesin-dockerin complex. *Proc Natl Acad Sci U S A* (2006)**,** *103*, 305-10.
(33)Ceccarelli, C.; Liang, Z.-X.; Strickler, M.; Prehna, G.; Goldstein, B. M.; Klinman, J. P.; Bahnson, B. J., Crystal Structure and Amide H/D Exchange of Binary Complexes of Alcohol Dehydrogenase from Bacillus stearothermophilus: Insight into Thermostability and Cofactor Binding. *Biochemistry* (2004)**,** *43*, 5266-5277.
(34)Lyskowski, A.; Gruber, C.; Steinkellner, G.; Schurmann, M.; Schwab, H.; Gruber, K.; Steiner, K., Crystal structure of an (R)-selective omega-transaminase from Aspergillus terreus. *PLoS One* (2014)**,** *9*, e87350.
(35)Alonso Villela, S. M.; Kraïem, H.; Bouhaouala-Zahar, B.; Bideaux, C.; Aceves Lara, C. A.; Fillaudeau, L., A protocol for recombinant protein quantification by densitometry. *MicrobiologyOpen* (2020)**,** *9*, e1027.
(36)Adler, J.; Parmryd, I., Quantifying colocalization by correlation: The Pearson correlation coefficient is superior to the Mander's overlap coefficient. *Cytometry Part A* (2010)**,** *77A*, 733-742.
(37)Dubey, N. C.; Tripathi, B. P., Nature Inspired Multienzyme Immobilization: Strategies and Concepts. *ACS Applied Bio Materials* (2021)**,** *4*, 1077-1114.